

Designing a Hydrogen Peroxide Biosensor Using Catalase and Modified Electrode with Magnesium Oxide Nanoparticles

Leili Aghebati-maleki¹, Bahareh Salehi², Rezvan Behfar³, Hajar Saeidmanesh⁴, Fereshte Ahmadian⁵, Mohammadtaghi Sarebanhassanabadi⁶, Masoud Negahdary^{6,*}

¹ Immunology Research Center, Tabriz University of medical sciences, Tabriz, Iran

² Department of Microbiology, Faculty of Biological Sciences, Islamic Azad University, North Tehran Branch, Tehran, Iran

³ Doroud University of applied science and technology, Doroud, Iran

⁴ Department of chemistry, Yazd Branch, Islamic Azad University, Yazd, Iran

⁵ Faculty of medicine, Shahid Sadoughi University of medical sciences, Yazd, Iran

⁶ Yazd Cardiovascular Research Center, Shahid Sadoughi University of Medical Sciences, Yazd, Iran

*E-mail: Masoud.negahdary@hotmail.com

Received: 18 July 2013 / Accepted: 25 September 2013 / Published: 15 November 2013

In this study a combination of biology, electrochemistry and nanotechnology was used in designing a biosensor capable of detecting hydrogen peroxide (H₂O₂) using a modified carbon paste electrode (CPE) with magnesium oxide nanoparticles (MgO NPs) and catalase (CAT) enzyme. Synthesized MgO NPs were studied by Ultraviolet-Visible Spectroscopy (UV-VIS), X-Ray Diffraction (XRD), and Transmission Electron Microscope (TEM). All electrochemical studies were conducted using Cyclic Voltammetry (CV). Results revealed that the CAT/MgO NPs/CPE complex produced a pair of well-defined redox peaks with formal potential $E^0 = 100 \pm 2$. The existence of Fe (III/II) structure in CAT molecule was an important factor that allowed the enzyme to participate in iron (Fe (III/II)) oxidation-reduction reactions; and these reactions that made it possible to design a biosensor for detecting H₂O₂. The designed biosensor was able to detect H₂O₂ in the range of 50-190 μ M. also designed biosensor has a high degree of stability and retained 92% of its original activity after a given duration.

Keywords: Bioelectrochemistry, Magnesium Oxide Nanoparticles, Catalase, Hydrogen Peroxide.

1. INTRODUCTION

Alongside the advancement of science and technology across the world, the number of scientific terminology is increasing day by day. Meanwhile, development of the science and

nanotechnology and its interaction with biology and electrochemistry has resulted in generation and application of terms such as bionanotechnology or nanoelectrochemistry in talks and works of researches all over the world. Nanotechnology is a novel technology that has captured the whole world. To put it more precisely, nanotechnology is not part of the future; rather, it forms the whole of it. It deals with the study of particles in atomic scale in order to control them. The main objective of most research works in the field of nanotechnology is to create new compounds or to bring about changes in existing materials [1-3]. The technology of nano is not a science in its own right, but it can be used to make various sciences applicable [4-5]. The range of research and study of materials and their properties in nanotechnology is 1-100 nm [6]. When materials are examined in the scale of nano, reactions of atoms and their behavior is significantly different from when this study is done at the level of molecules, since in nano-scale physical properties of materials change [7-8]. Compared to nanomaterials that have bigger particles, those with smaller particles have greater surface area per unit of mass. Given the greater surface of these materials, their contact with other elements is increased which leads to more reactions with them [9-10]. In fact, these materials are capable of interacting with various chemical groups in order to increase their affinity for certain compounds. Nanoelectrochemistry is a branch of electrochemistry that is involved with the study of electrical and electrochemical properties of materials in the range of nanometer. Nanoelectrochemistry plays a significant role in producing various sensors and instruments used for the detection of molecules at very low concentrations [11]. Particular characteristics of nanostructures and their application in electrochemistry have resulted in the improvement of electrochemical sensors' operation [12-14]. Today sensors provide us with lots of information about heat, temperature, weather conditions, earth, sea transportation, chemical pollutants and biological substances [15-16].

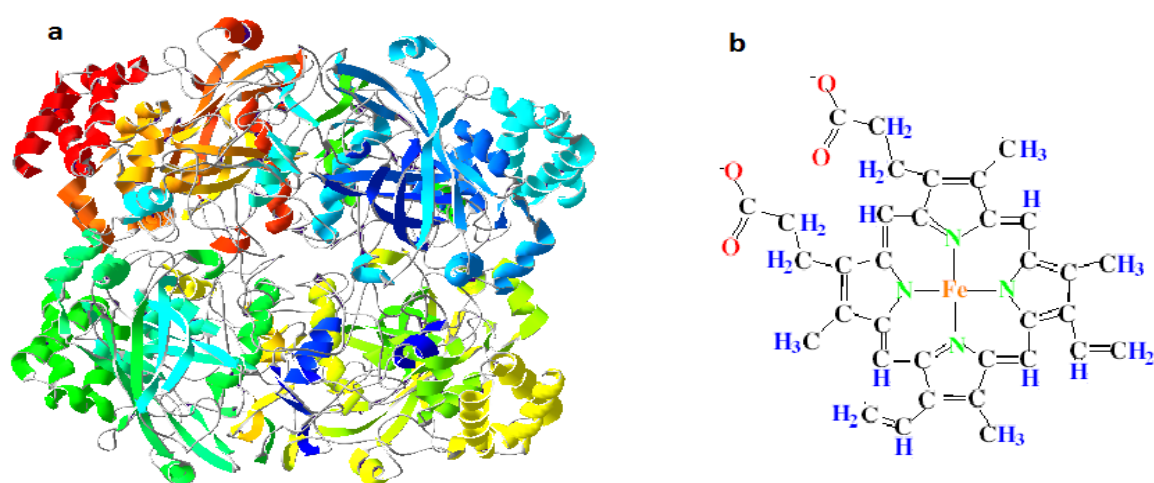


Figure 1. CAT Enzyme; (a) Molecular Structure, (b) Chemical Structure

Nanotechnology has made it possible for the sensors to increase their sensitivity and decrease their detection time. Biosensors are defined as a group of sensors which have biological components in their structure. One of the ultimate goals of direct electron transfer in protein structures is to design

diagnostic sensors to detect different materials in very small concentrations [17-18]. The protein structure used in this research was CAT enzyme. As is already known, enzymes act as catalysts; that is to say, they accelerate reaction rate without themselves undergoing any changes [19]. CAT is an antioxidant enzyme found in most aerobic cells. It has a dumbbell-shaped structure with four polypeptide chains, each over 500 amino acids long. It also contains four heme groups which can take part in oxidation-reduction reactions by means of electron transfer [20-21]. Figure 1 (a & b) shows molecular and chemical structures of CAT.

The important function of CAT is to decompose H_2O_2 to water and oxygen molecules [22]. In this study we used of MgO NPs as facilitator and accelerator of electron-transfer. Enzyme-Modified electrodes are simple tools based on the coupling of an enzyme and an electrochemical transducer. Using enzymes' functional specificity and electrochemical transducers' ability to transfer signals, these electrodes are capable of detecting various analytes [23-24]. Generally speaking, electrochemical sensors employed in the laboratories of pharmaceutical, medical, chemical, environmental, defense, water and waste-water industries take benefit from these electrodes [25-27]. Carbon-paste electrodes are easy to synthesize at a very low price; they also have long life-span. Compared to other electrodes, those prepared in this research have several advantages, such as their relatively low price, being non-poisonous, simplicity of preparation, broad range of applicable potential, quick response, freedom from mechanical damage, high capacity for modify, and their renewable surface, to mention just a few [28-30]. Considering the crucial role H_2O_2 has in medical and environmental studies as well as industrial processes, its determination is of great importance [31-32]. Furthermore, H_2O_2 is one of the important by-products of oxidative enzymes and its determination allows for the substrates of these enzymes to be assessed [33]. In this research the aim was to assess and measure H_2O_2 in solutions, and the ability of the prepared enzyme electrode in the quantitative detection of H_2O_2 was examined.

2. EXPERIMENTAL

2.1. Materials

CAT enzyme isolated from human liver (50 unit/g) was purchased from Sigma. Graphite powder and paraffin required for preparing carbon-paste electrodes, as well as raw materials needed for phosphate buffer solution 0.1 M (pH. 7), including disodium monohydroxy phosphate (Na_2HPO_4) and monosodium dihydroxy phosphate (NaH_2PO_4), were all obtained from Merck. For preparing MgO NPs we used Magnesium Acetate [$Mg(CH_3COO)_2$] 0.14 M, Poly Vinyl Pyrrolidone [$(C_6H_9NO)_n$], Trimethyl Ammonium Hydroxide [$(CH_3)_4NOH$] and Ethanol [C_2H_6O], all purchased from Merck. In all electrochemical tests double distilled deionized water was used, as otherwise ions existing in water would be likely to interfere with direct electron transfer processes. Other materials and tools used in the laboratory were obtained from reputable companies.

2.2. Apparatus

In the electrochemical cell employed in the research, we used a three-electrode system which consisted of (1) a bare or MgO NPs-modified carbon-paste electrode (4 mm diameter), as the working

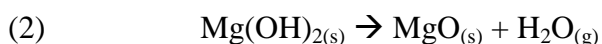
electrode, (2) a saturated calomel electrode (SCE) as the reference electrode, and (3) a platinum electrode as the counter electrode. It must be added that saturated calomel and platinum electrodes were purchased from Azar-Electrode Company, Urmia, Iran. Electrochemical experiments were conducted by CV using an EA-201 Electro-Analyzer manufactured by Chemilink Systems Co. This device was connected on one side to the three electrodes mentioned above, and on the other side it was equipped with a personal computer to analyze data and plot oxidation-reduction diagrams. Morphologic studies and examination of the surface of synthesized MgO NPs were performed by devices of a TU-1901 double-beam UV-visible spectrophotometer, a D/Max-RA X-ray diffractometer using CuK α radiation, and a JEM-200CX TEM.

2.3. Preparation of MgO NPs

To prepare MgO NPs, 50 ml magnesium acetate solution (0.14 M) was sonicated with required amounts of PVP as the structure-control factor for 30 minutes, and then sufficient volume of trimethyl ammonium hydroxide (TMAH) solution (0.34 M) was slowly added to it. At this step magnesium hydroxide nanostructure was formed through the following reaction:



At the end of the process of adding TMAH, the obtained mixture was sonicated for 30 minutes. The precipitated magnesium hydroxide was filtered and then washed three times with distilled water and ethanol. Ethanol (50 ml) was added to the obtained precipitate and the mixture was again sonicated for 30 minutes and then filtered. The final obtained precipitate was dehydrated at 550° C for 4 hours. The following reaction shows the step of magnesium dehydration:



In order to remove its agglomerated state, MgO NPs were sonicated in ethanol for 30 minutes. In the last step, the resultant mixture was filtered and dried at 110° C. The final product, powdery in form, was MgO NPs that was to be used in later steps of the research.

2.4. Preparation of Bare Carbon-Paste Electrodes

In order to prepare a bare CPE, carbon powder (particle size 50 mm, density 20-30 gr/100 ml) was mixed with binders and silicone oil into a paste in an agate mortar, and was homogenized in a pestle. An electrode consisting of high-quality Teflon was placed at the end of a Teflon tube and then the paste prepared in the previous stage was packed into the tube. A copper wire ran through the paste so that the carbon-paste electrode could establish an electrical connection with an external circuit. Before this electrode was used in electrochemical studies, it was refined mechanically using some paste prepared as described above, and then was polished by a piece of transparent paper.

2.5. Preparation of Modified CPE with MgO NPs

To prepare MgO NPs-modified CPE, carbon powder, binders and 10 mg MgO NPs were mixed with silicon oil in an agate mortar to make carbon paste. The remaining steps were similar to the

procedure used for preparing bare CPE.

2.6. Preparation of Modified CPE with MgO NPs and CAT

MgO NPs /CPE made in previous stage were used to prepare Modified CPE with both MgO NPs and CAT. At this step CAT was immobilized on the surface of MgO NP/CPE by pouring 2 μ l of protein solution 10 mg/ml and was dried at room temperature in 30 minutes. Then the prepared electrode was gently washed with double-distilled water, and was kept in refrigerator at 4° C when not in use.

3. RESULTS AND DISCUSSION

3.1. Examining Properties of Synthesized MgO NPs

3.1.1. XRD Pattern of Produced MgO NPs

XRD that takes place by a group of atoms is resulted from the reinforcement of diffracted rays in certain directions. When an X-ray beam hits electrons of a matter, it makes them oscillate; these electrons, in turn, make the X-ray beam radiate into the space around with the same frequency as the original (incident) beam [34]. If the scattered beams are combined, a resultant wave will be generated whose amplitude depends on the number of electrons and phase-difference of reflected waves. This phase-difference depends on the different directions taken by rays. Rays reflected by various atoms will have different phases due to the different directions they will take, and this phase-difference will lead to the amplitude of the rays reflected from the group of atoms to be varied. Since intensity of a ray is in proportion to the second power of its amplitude, changes in the directions taken by various rays result in differences in their amplitudes. Therefore, in certain cases when amplitudes of rays are added to each other, the ray reflected from the group of atoms is enhanced, a phenomenon called “XRD”. To understand this we need to notice that, in most cases, the spacing is not suitable and therefore amplitudes are not added. As a result, rays scattered from the group of atoms weaken each other, and this leads to the intensity of the final ray being negligible. In an XRD device the X-ray is radiated from the ray-generating tube onto an unknown specimen and the intensity of diffracted rays is measured at various angles; thus, the function of the diffractometer is to determine the angles at which diffraction takes place according to Bragg’s Equation ($2d\sin\theta = n\lambda$)[35]. Figure 2 shows the XRD pattern of MgO NPs. Diffraction peaks have been absorbed at 2θ values. The prominent peaks were utilized to estimate particle size of the sample with the help of Scherrer’s Equation, $D=K\lambda/(\beta\cos\theta)$, in which K is constant (equal to 0.9), λ is the wavelength ($\lambda = 1.5418 \text{ \AA}$) (Cu K α), β is the full-width at the half-maximum of the line, and θ is diffraction angle. The size of particles estimated using the relative peak intensity was found to be 70 nm for MgO NPs, and increase in the sharpness of XRD peaks indicated that particles were crystalline in nature.

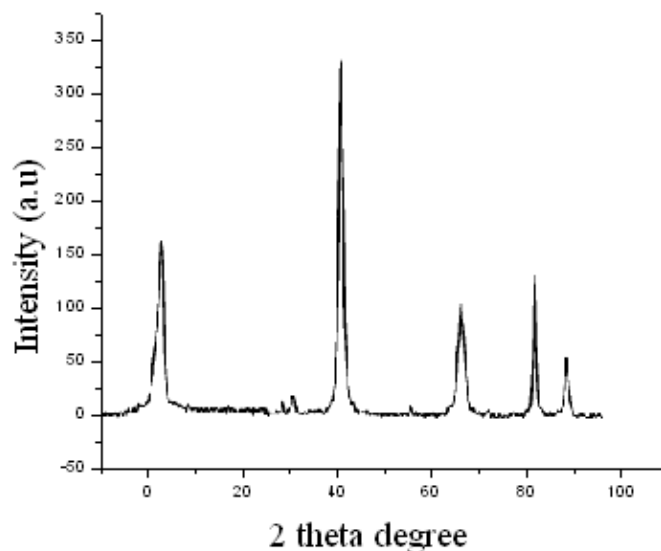


Figure 2. XRD pattern for synthetic MgO NPs

3.1.2. Characteristics of UV-VIS Spectroscopy of MgO NPs

This spectroscopy is related to the transition between energy levels (electron states). Such transitions generally take place between the bonding-orbital or non-bonding electron pairs with the anti-bonding orbital; therefore it is possible to associate wavelength of absorption peaks with various bonds existing in the sample under study [36-37]. In Figure 3 be shown a UV-VIS spectroscopy of chemically-synthesized MgO NPs. As shown here, the absorption peak is located in the area of 220-650 nm. The fact that the peak is not sharp indicates that nanoparticles with different sizes are produced in this method. The results of UV-VIS spectroscopy confirmed the data obtained by electron microscopy and proved particular and quantum properties of nanoparticles.

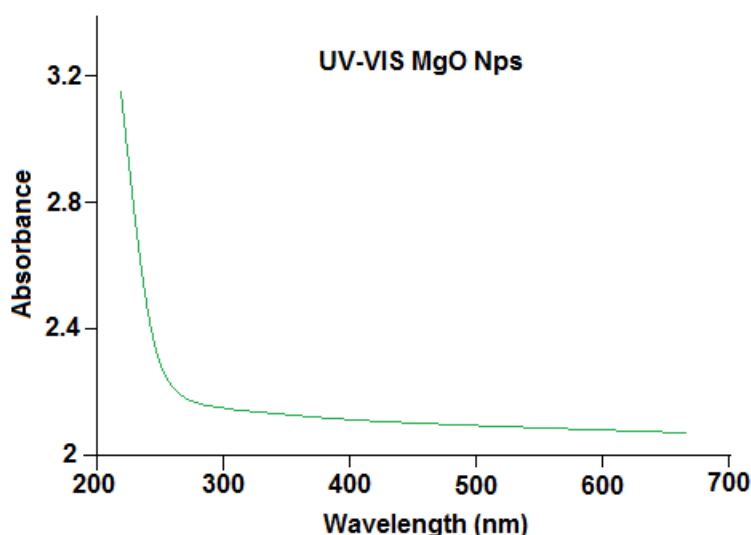


Figure 3. UV-VIS spectrum of synthesized MgO NPs

3.1.3. Electron Microscope Examination of MgO NPs

Though the TEM operates on the same basic principles as the light microscope, yet in the former (i.e. the TEM) rays come from above down. This electron microscope consists of a long column on top of which the source of electron rays is mounted. After transmitting through the specimen, electron rays hit a photographic film or screen (built of fluorescent materials) and create an image [38]. Since some rays do not pass through the sample, black spots are left on the image and therefore electron microscope images are black-and-white. Slices in a TEM are much thinner than those in a light microscope, and staining techniques also are different. In Figure 4 a TEM image of synthesized MgO NPs is seen. The smaller the size of nanoparticles, the greater their surface area-to-volume ratio; thus, these nanoparticles can play a key role during immobilization processes. According to the results obtained from TEM studies, the size of synthesized MgO NPs was estimated 70 nm.

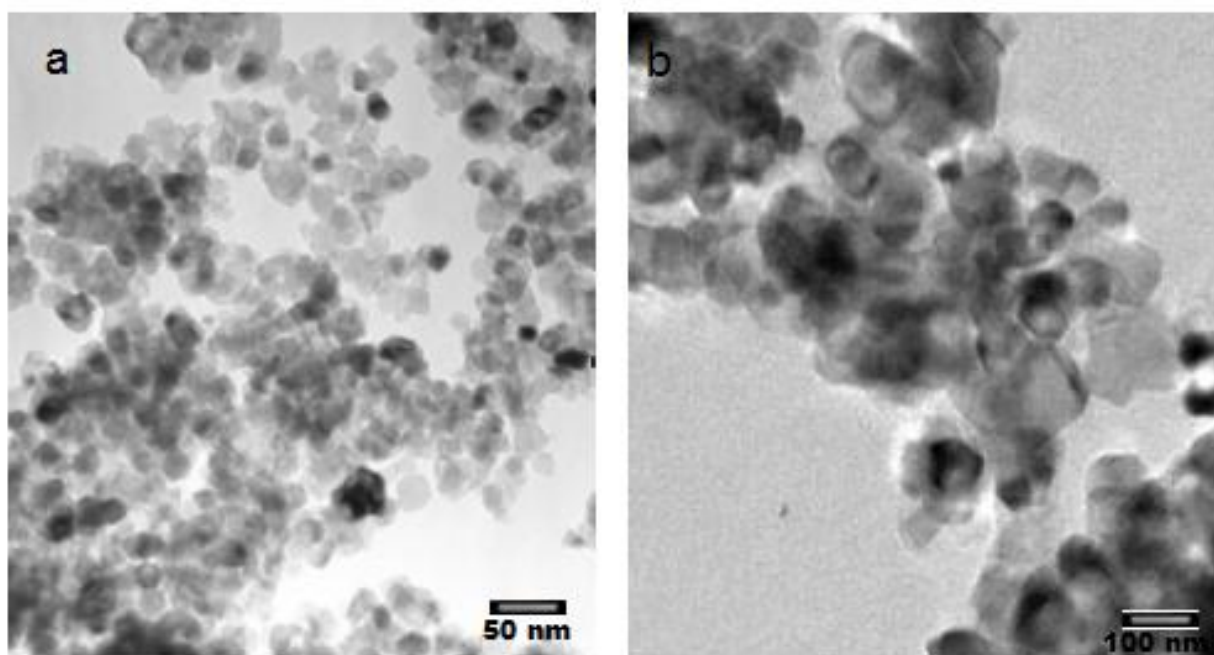


Figure 4. TEM image of synthesized MgO NPs

3.2. Direct Electron Transfer from CAT to the Surface of MgO NPs /CPE, and Vice Versa

At this part cyclic voltammogram studies were conducted in order to find and examine oxidation and reduction peaks in CAT/MgO NPs /CPE. Another important aim of this section was to determine the difference in the functioning of bare electrodes compared to those modified with MgO NPs and CAT. Figure 5 depicts the cyclic voltammogram related to the three-electrode system in phosphate buffer solution (PBS) 0.1 M at pH. 7. The working electrode in this research was CPE considered in four different conditions. All electrochemical studies were conducted against saturated calomel electrode (SCE) as the reference electrode. Scan rate in this part of research was 50 mV/s^{-1} . In the first condition, bare CPE (modified with neither MgO NPs nor CAT) was studied in which case no

oxidation (anodic) or reduction (cathodic) peaks were observed; This conditions has been depicted in Figure 5-a. Secondly, the CPE was modified only with MgO NPs and again no oxidative/reductive (redox) peaks were seen (not shown here). The third observation was done using CAT-modified CPE. Here a pair of oxidative/reductive peaks was seen which indicated CAT response to carbon-paste electrode, however the peaks were very small and inefficient (not shown here). Finally, in the last and the most important case, CAT/MgO NPs /CPE was used and a pair of well-defined and efficient peaks was obtained. The height of peaks in this case was such that it could be regarded as a target in terms of electrochemical research. This condition has been shown in Figure 5-b. Anodic and cathodic peaks were located at 160 mV and 40 mV, respectively (Versus. SCE), which is indicative of stable immobilization of CAT and MgO NPs on the surface of CPE. Here the role of MgO NPs is to facilitate and accelerate electron transfer rate between heme group of CAT and CPE. Formal potential, denoted by E^0 , was obtained from the average potential of anodic and cathodic peaks and its value was estimated here to be 100 ± 2 . In our previous study using CAT / CdO NP/ CPE, the value -155 was obtained for E^0 [39].

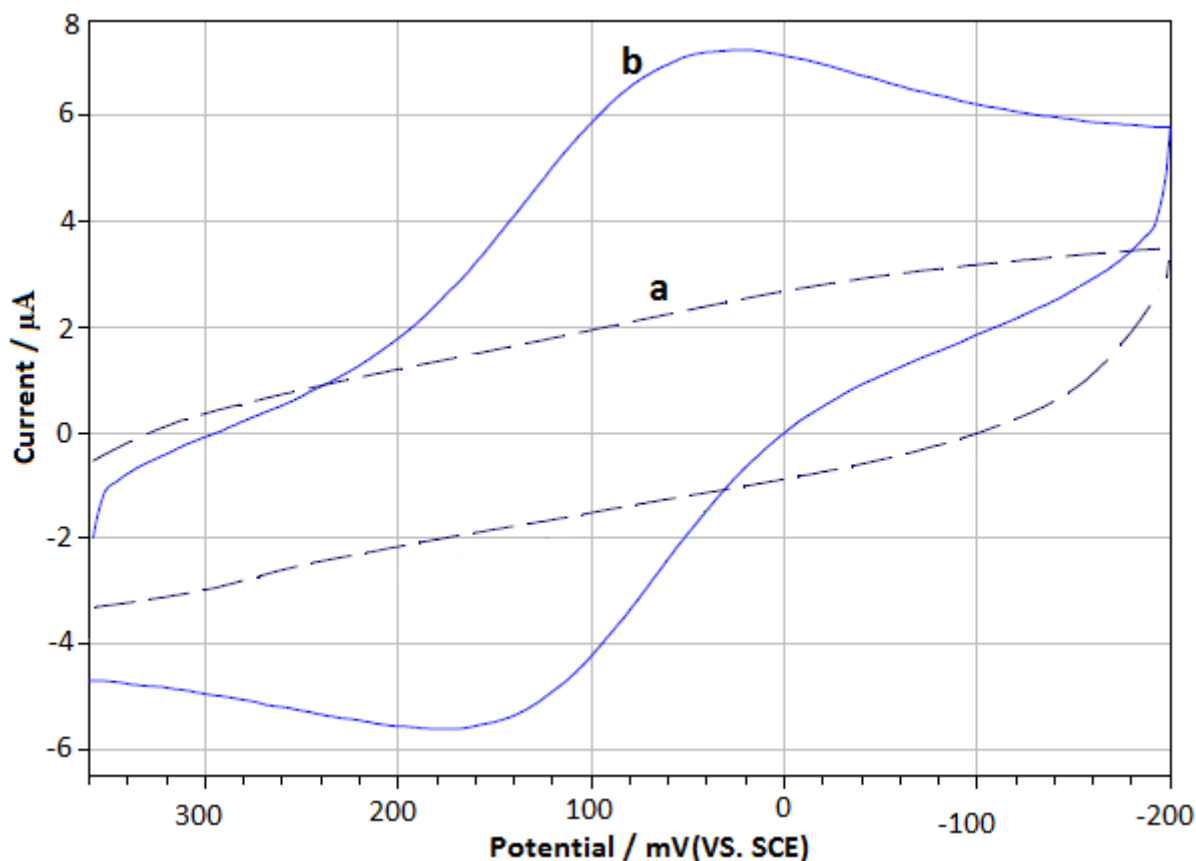
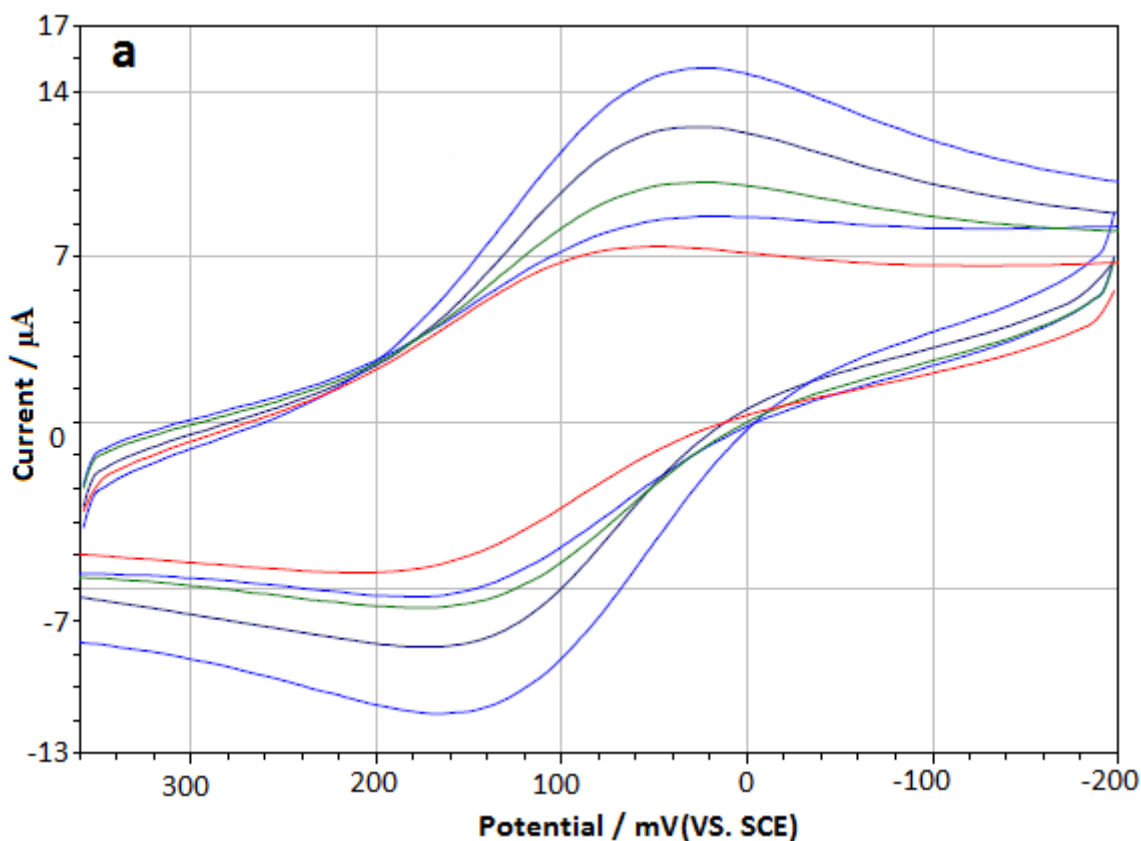


Figure 5. Cyclic voltammogram, (a) bare CPE,(b) CAT/MgO NPs /CPE; Scan rate 50 mV/s^{-1} , in 0.1 M phosphate buffer solution at pH 7.0.

Next, CAT/MgO NPs /CPE was considered in PBS (0.1 M, pH 7.0) at various scan rates (50, 100, 200, 300 and 400 mV/s^{-1}). As can be seen in Figure 6, parallel to the increasing values of scan rate, the height of redox peaks also increase. Unfortunately, for some reasons direct electron transfer

by means of enzymes is very difficult. For example it is plausible that enzymes be attracted to the surface of electrode through hydrophobic bonds; this causes enzyme molecules to become abnormal and therefore lose their electrochemical activity. Other factors such as complicated three-dimensional structures, redox center being located deep inside the enzyme, and lack of ready access to the enzymes' active site render direct electron transfer via enzymes more difficult. However, since in this study nanoparticles were used, given the fact that they have greater surface-to-volume ratio, so their reactivity was much more than their bulk state. This fact led to meaningful increase in the rate of electron transfer between CAT heme group and CPE [10-12]. To analyze this part of electrochemical studies in more detail, the data obtained from Figure 6-(a) were plotted in the form of special diagrams in Figures 6-b (based on scan rate, ν) and 6-c (based on square root of scan rate, $\nu^{1/2}$). It is seen that redox peaks show a linear increase and the obtained correlation coefficient for cathodic and anodic peaks are equal to 0.9879 ($i_{pc} = 0.0238 \nu + 6.6335$) and 0.9899 ($i_{pa} = -0.0179 \nu - 4.4588$), respectively. These values confirm proper and stable immobilization of CAT on the surface of carbon-paste electrode and also effective role of MgO NPs as facilitators of direct electron transfer process. Besides, findings of this part showed that the diagram in Figure 6-b has a more linear nature than that in Figure 6-c. Results of this part of studies can be used to determine the amount of CAT in phosphate buffer solution.



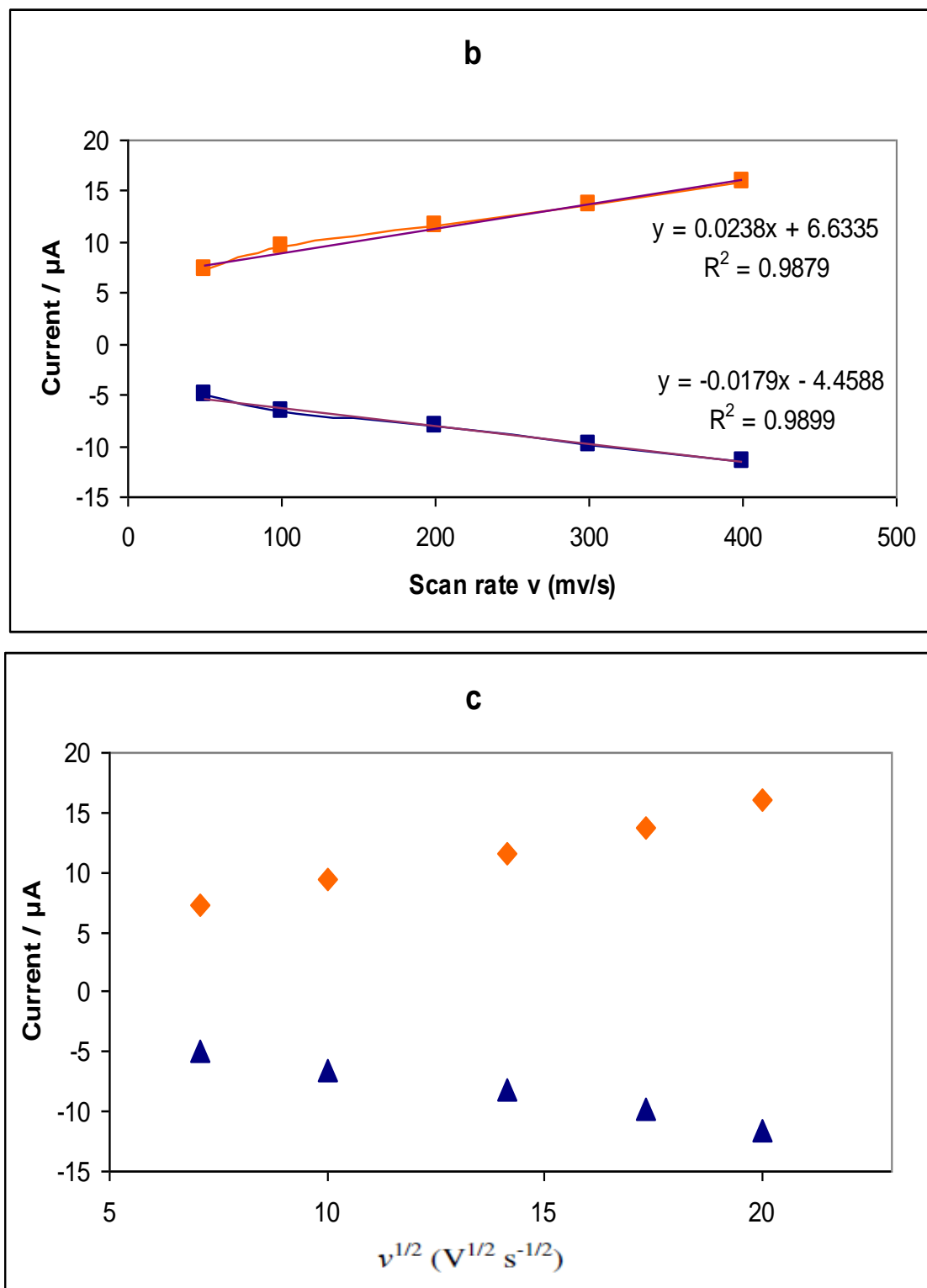


Figure 6. (a) Cyclic voltammograms of CAT/MgO NPs/CPE; (b) Line gradient and equation and diagram plotted on the basis of scan rate; (c) Line gradient and diagram plotted on the basis of square root of scan rate; Scan rate increasing from lowest value of 50 mV/s^{-1} to 100, 200, 300 and 400 mV/s^{-1} in 0.1 M phosphate buffer solution at pH 7.0.

Existence of $\text{Fe}_{(\text{III/II})}$ structure in CAT is an important factor that allows the enzyme to

participate in electrochemical, particularly oxidation/reduction, reactions. All such reactions involve electron transfer in which $\text{Fe}_{(\text{III})}$ is the oxidative form whereas $\text{Fe}_{(\text{II})}$ is in the reductive state. Where peak-to-peak separation, or energy difference (ΔE), is greater than 200 mV, electron-transfer coefficient (k_s) can be obtained easily through Laviron Equations mentioned below [40-41]:

$$E_{p, \text{cathodic}} = E^0 + \frac{RT}{\alpha F} \ln \frac{RTk_s}{\alpha Fv} \quad (3)$$

$$E_{p, \text{anodic}} = E^0 + \frac{RT}{(1-\alpha)F} \ln \frac{RTk_s}{(1-\alpha)Fv} \quad (4)$$

$$\Delta E_p = E_{p, \text{anodic}} - E_{p, \text{cathodic}} = \frac{RT}{\alpha(1-\alpha)F} \quad (5)$$

$$\left[\log k_s = \alpha \log(1-\alpha) + (1-\alpha) \log \alpha - \log \frac{RT}{nFv} - \frac{\alpha(1-\alpha)nF\Delta E_p}{2.3 RT} \right] \quad (6)$$

where α is the electron-transfer coefficient and n indicates the number of transferred electrons. R , F and T are gas constant, Faraday constant and absolute temperature, respectively, all having definite values:

$$R = 8.314 \text{ J mol}^{-1} \text{ K}^{-1}, \quad F = 96493 \text{ C/mol}, \quad T = 298 \text{ K}$$

The electron transfer rate constant (k_s) can be obtained by means of ΔE_p in terms of $\ln v$. In this study, $k_s = 1.40 \text{ s}^{-1}$ and $\alpha = 0.52$ were calculated. In a research conducted by Wu, et al on direct electron transfer in CAT with silk fibroin (SF), $k_s = 0.34 \text{ s}^{-1}$ was obtained [42]. In another study performed by the authors of the present research CAT /CdO NP/CPEs was used and we reached at $k_s = 1.23 \text{ s}^{-1}$ [39]. In still another work Zhou, et al employed multi-walled carbon nanotubes (MWCNTs), CAT and glassy carbon electrode and estimated the value of electron transfer rate constant to be $k_s = 1.07 \text{ s}^{-1}$ [43]. Greater numeric values for k_s suggest that CAT/MgO NP/CPEs have an increased rate of electron transfer between CAT and the CPE.

3.3. Effect of pH on Formal Potential (E^0) of a CAT/MgO NPs/CPE

In the next phase of the study the effect of electrolyte pH on modified CPE with MgO NPs and CAT was examined and it was observed that changes in PBS-pH in the range of 4 to 9 results in a negative shift in redox peaks potential of CAT/MgO NPs/CPE. Results of this part in terms of formal potential E^0 are shown in Figure 7. In this part of study correlation coefficient of 0.9972 was obtained and line gradient was estimated to be -30 mV. Maximum activity and optimal state of PBS was observed at pH 7.0, and this was the reason why in subsequent studies also we used PBS at pH 7.0. Calculations of this part were very close to the grounded theory on the participation of a protein structure in electron-transfer reactions [44].

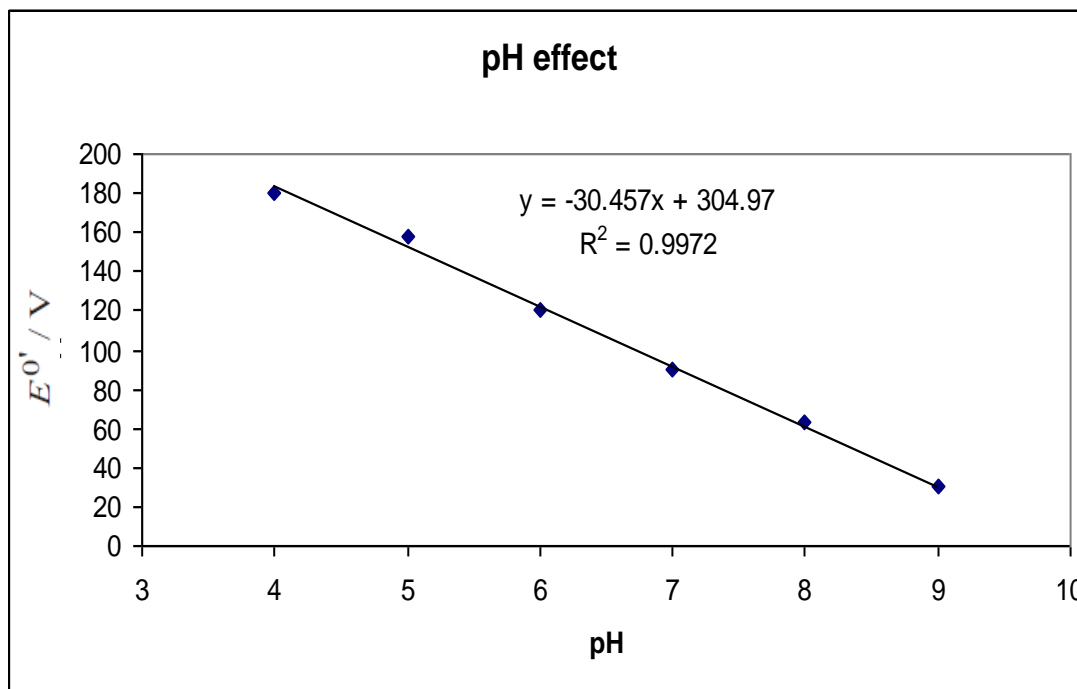


Figure 7. Linear association of formal potential and solution pH for modified CPE with CdO NPs and CAT (0.1 M PBS, scan rate of 50 mV/s^{-1})

3.4. Designing a Biosensor to Detect H_2O_2 using CAT/MgO NPs/CPE

The importance of detecting H_2O_2 in ranges as small as μM concentrations in biological, medical and industrial activities is quite obvious. In detecting H_2O_2 various methods of spectrometry, chemiluminescence and electrochemistry are employed [45]; yet a more suitable and efficient choice is electrochemical processes, as they offer greater sensitivity and selectivity compared to other methods. In present research various concentrations of H_2O_2 were added in the presence of CAT/MgO NPs/CPE to PBS (0.1 M) at pH. 7, and cyclic voltammetric studies (Versus SCE) were performed. Results revealed that as concentration of H_2O_2 is increased, the height of cathodic peak also increases while that of anodic peak is decreased. These findings are seen in Figure 8-(a). In this section of the research it was found out that sensitivity and reactivity to H_2O_2 happens only when all the three factors (i.e., CPE, MgO NPs and CAT) are used together. The electrocatalytic response which leads to the oxidation-reduction reaction in the designed biosensor can be expressed as below:



Such a process provides firm evidence for the catalytic effect of CAT and its proper immobilization on the surface of CPE, where the process of electron transfer has been facilitated by MgO NPs. Our designed biosensor is capable of detecting H_2O_2 in the range of 50-190 μM . In another research Salimi et al, used CAT and modified electrodes with NiO NPs to detect H_2O_2 , and their biosensor could detect H_2O_2 in the concentrations of 0.001-1 mM [46]. In still another study conducted by us, we employed CAT/CdO NP/CPE and were able to detect H_2O_2 in the range of 25-210 μM [39].

In Figure 8-b calibration curves related to the biosensor designed to detect H_2O_2 using CAT and MgO NPs have been shown. Correlation coefficient in this part of the study was 0.9981. Cathodic peak growth is stopped at the highest concentration of H_2O_2 and reaches a stable value at $190 \mu\text{M}$, which is the maximum reaction of our designed biosensor to H_2O_2 . Details are depicted in Figure 8-(b).

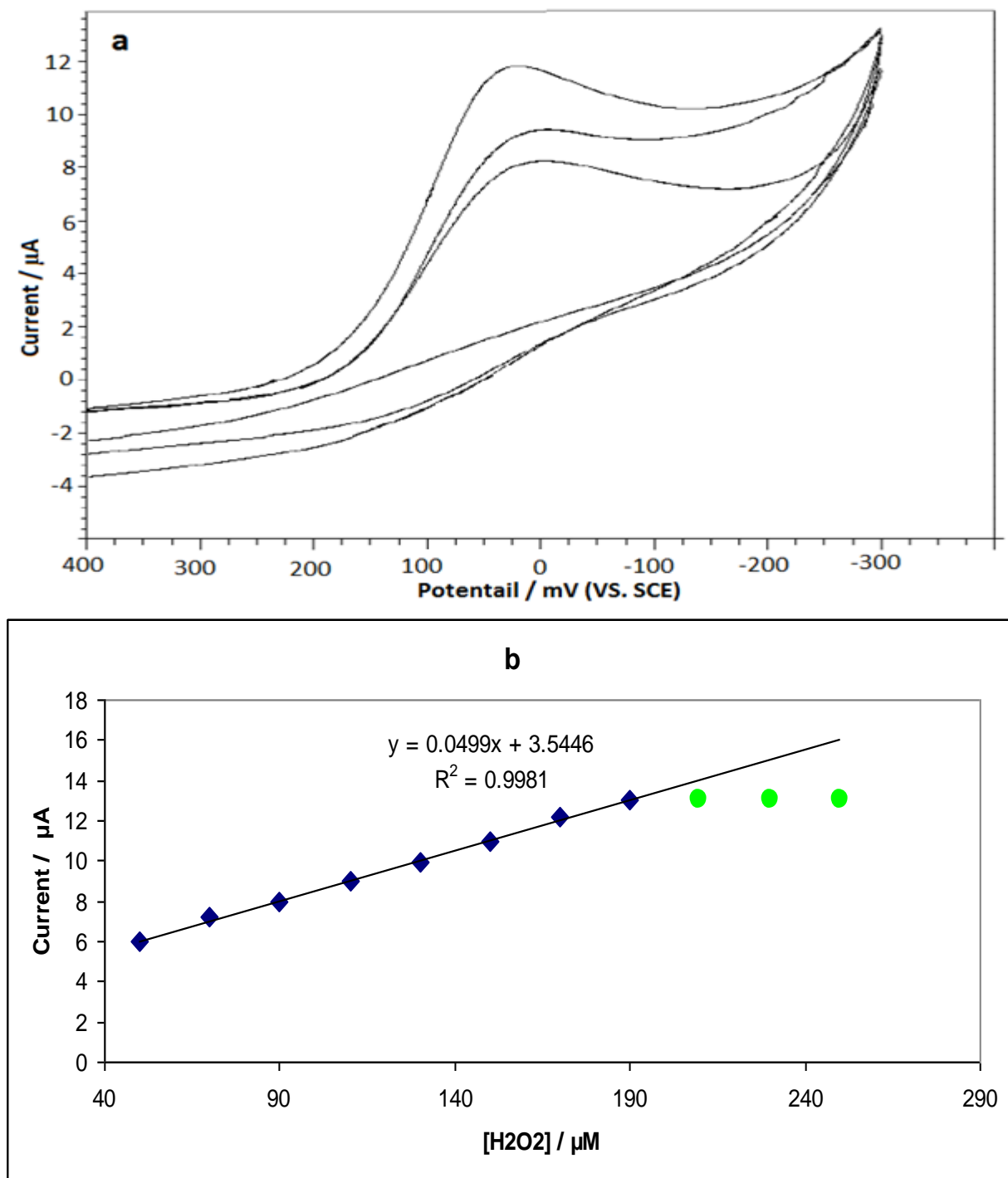


Figure 8. (a) Cyclic voltammograms of CAT/MgO NPs/CPE at various concentrations of H_2O_2 ; (b) The relationship between CAT cathodic peak current and different concentrations of H_2O_2 (scan rate of 50 mV/s^{-1} , 0.1 M PBS , $\text{pH } 7.0$)

3.5. Stability of Biosensor Designed to Detect H₂O₂

The designed biosensor for detecting H₂O₂ using modified CPE with CAT and MgO NPs was also studied in terms of its stability. Considering the fact that an enzyme structure was employed in this research, one crucial factor in preserving stability of the biosensor was to prevent denaturation of the enzyme. Initial activity and reaction rate of the biosensor was measured for 30 days until it reached a stable value. To test its stability, the biosensor was kept in the fridge at 3° C for 50 days; given the reduction of enzyme activity due to the mechanical damage to its structure, our designed biosensor retained 92% of its initial activity after this duration. It was also observed that our biosensor has high reproducibility, and that interfacing factors had no important effect to reduce its functioning.

4. CONCLUSION

Convergence of nanotechnology with biology and electrochemistry has resulted in the design and manufacture of more efficient biosensors. Considering the importance of detecting and measurement of H₂O₂ we decided to design a new sensor of the third generation to detect this substance. In the design of the said biosensor, basic applications and interaction of nanotechnology, biology and electrochemistry is quite manifest. Among the features of the biosensor designed in this research its high stability, reasonable reproducibility, and not being affected by interfacing substances are worth mentioning.

References

1. J.J. Ramsden, *Nanotechnology Perceptions*, 1 (2005) 3.
2. Geoffrey A. Ozin, Ludovico Cademartiri, *Small*, 5 (2009) 1240.
3. P.A. Revell, *Nanotechnology Perceptions*, 2 (2006) 283.
4. S. de Haan, *Nanotechnology Perceptions*, 2 (2006) 267.
5. P. Schaaf and J. Talbot, *J. Chem. Phys.* 91 (1989) 4401.
6. P.A. McKeown, J. Corbett, P. Shore and P. Morantz, *Nanotechnology Perceptions*, 4 (2008) 5.
7. A.G. Mamalis, A. Markopoulos and D.E. Manolakos, *Nanotechnology Perceptions*, 1 (2005) 63.
8. Politi and J.L. O'Brien, *Nanotechnology Perceptions*, 4 (2008) 289.
9. M. Tristany, M. Moreno-Manas, *New J. Chem.*, 33 (2009) 1529.
10. A.P. Alivisatos, P.F. Barbara, *Adv. Mater.*, 10 (1998) 1297.
11. Cao, X.; Ning, W.; Li, L. D. & Guo, L. *Sensors and Actuators B-Chemical*, 129 (2008) 268.
12. Cui, H. F.; Ye, J. S.; Zhang, W. D. & Sheu, F. S. *Biosensors and Bioelectronics*, 24 (2009) 1723.
13. Duan, G. P.; Li, Y. F.; *Electroanalysis* 20 (2008) 2454.
14. Ansari, A.A.; Sumana, G.; Khan R.; Malhotra, B.D., *J. of Nanosc. and Nanotechnology*, 9 (2009) 1.
15. S. Rezaei-Zarchi, M. Negahdary, *Advances in Environmental Biology*, 5 (2011) 3241.
16. Gholamreza Mohseni, Masoud Negahdary, Hossein Faramarzi, *Int. J. Electrochem. Sci.*, 7 (2012) 12098.
17. Masoud Negahdary, Seyedeh Anousheh Sadeghi, *Int. J. Electrochem. Sci.*, 7 (2012) 6059.
18. Masoud Negahdary, Asadollah Asadi. *Int. J. Electrochem. Sci.*, 7 (2012) 5185.
19. Bennett, T. P., and Frieden, E.: *Modern Topics in Biochemistry*, Macmillan, London, (1969).
20. Periasamy, A.; Umasankar, Y.; and Shen-Ming, Ch. *Sensors*, 9 (2009) 1821.

21. Buleandra, M.; Radu, G.L; Tanase, I. *Biotechnol. Lett*, 5 (2000) 423.
22. Lai, M.E.; Bergel, A. *Bioelectrochemistry*, 55 (2002) 157.
23. Lu, H.Y.; Li, Z.; Hu, N.F. *Biophys. Chem*, 104 (2003) 623.
24. Li, Y.M.; Chen, X.T.; Li, J.; Liu, H.H.; *Electrochim. Acta*, 49 (2004) 3195.
25. Scheller, F. W.; Schubert, F.; Fedrowitz, J. *EXS*, 80 (1997) 1.
26. Rocchitta, G.; Migheli, R.; *Sens. Actuat. B*, 126 (2007) 700.
27. Drummond, T. G.; Hill, M. G. & Barton, J. K. *Nat. Biotechnol*, 21(2003) 1192.
28. I. Švancara, R. Metelka and K. Vytřas, *Piston-Driven Carbon Paste Electrode Holders for Electrochemical Measurements*, University of Pardubice, Pardubice (2005).
29. Ivan S vancara a, Karel Vytrřas a, Andrzej Bobrowski, Kurt Kalcher. *Talanta*, 58 (2002) 45.
30. Matsubara, C.; Kawamoto, N.; Takamura, K. *Analyst* , 117 (1992) 1781.
31. Thanachasai, S.; Rokutanazono, S.; Yoshida, S.; Watanabe, T. *Anal. Sci* , 18 (2002) 773.
32. Hurdis, E.C.; Hendrik Romeyn, J. *Anal. Chem.*, 26(1954) 320.
33. Serradilla Razola, S.; Lopez Ruiz, *Biosens. Bioelectron*, 17(2002) 921.
34. Letizia Monico, Geert Van der Snickt, Koen Janssens, *Anal. Chem.*, 83 (2011) 1224.
35. Letizia Monico, Geert Van der Snickt, *Anal. Chem.*, 83 (2011) 1214.
36. L. Sooväli, E.-I. Rõõm, A. Kütt, *Accred. Qual. Assur*, 11 (2006) 246.
37. Skoog, et al. *Principles of Instrumental Analysis*. 6th ed. Thomson Brooks/Cole. (2007).
38. Alvarez, J. M. A.; Pineyro, *Review of Scientific Instrumentation* (1996).
39. Malekzadeh, R.; Negahdary, M.; Farasat, A.; Torkamani Noughabi, M.; *European Journal of Experimental Biology*, 2 (2012) 454.
40. Laviron, E.; *Journal of Electroanalytical Chemistry*, 101, (1979) 19.
41. Laviron, E.; *Journal of Electroanalytical Chemistry*, 100 (1979) 263.
42. Wu, Y.; Shen, Q.; Hu, S. *Anal. Chim. Acta* , 558 (2006) 179.
43. Zhou, H.; Lu, T.H.; Shi, H.X.; Dai, Z.H.; Huang, X.H. *J. electroanal. Chem* , 612 (2008) 173.
44. Wightman, R. M.; Wipf, D. O. *In Electroanalytical Chemistry*; Bard, A. J., Ed.; Marcel Dekker: New York, (1989).
45. Gholamreza Mohseni, Masoud Negahdary, *Int. J. Electrochem. Sci.*, 7 (2012) 7033.
46. Salimi, A.; Sharifi, E.; Noorbakhsh, A.; Soltanian, S. *Biophys. Chem*, 125 (2007) 540.